Turbulence and Bed Load Transport in Channels With Randomly Distributed Emergent Patches of Model Vegetation

Citation: Shan, Y., Zhao, T., Liu, C., & Nepf, H. (2020). Turbulence and bed load transport in channels with randomly distributed emergent patches of model vegetation. Geophysical Research Letters, 47, e2020GL087055

As Published: 10.1029/2020GL087055

Publisher: American Geophysical Union (AGU)

Persistent URL: https://hdl.handle.net/1721.1/133056

Version: Final published version: final published article, as it appeared in a journal, conference proceedings, or other formally published context

Geophysical Research Letters

RESEARCH LETTER
10.1029/2020GL087055

Key Points:
- Channel-averaged sediment transport decreased as the total stem number decreased and as stems were gathered into smaller patches (decreasing patch diameter)
- For both uniform and clustered (patch) distributions of stems, the channel-averaged sediment transport can be predicted from channel-averaged turbulence
- A model was developed to predict channel-averaged turbulence and sediment transport for randomly distributed stem patches

Supporting Information:
- Supporting Information S1

Correspondence to:
C. Liu,
liuchaoscu@vip.qq.com;
chaoliu@scu.edu.cn

Citation:
Shan, Y., Zhao, T., Liu, C., & Nepf, H. (2020). Turbulence and bed load transport in channels with randomly distributed emergent patches of model vegetation. *Geophysical Research Letters*, *47*, e2020GL087055. https://doi.org/10.1029/2020GL087055

Received 15 JAN 2020
Accepted 25 MAR 2020
Accepted article online 9 APR 2020

Turbulence and Bed Load Transport in Channels With Randomly Distributed Emergent Patches of Model Vegetation

Yuqi Shan[1,2,3], Tian Zhao[2], Chao Liu[2,3], and Heidi Nepf[2]

[1]College of Applied Mathematics, Chengdu University of Information Technology, Chengdu, China, [2]Department of Civil and Environmental Engineering, Massachusetts Institute of Technology, Cambridge, MA, USA, [3]State Key Laboratory of Hydraulics and Mountain River Engineering, Sichuan University, Chengdu, China

Abstract Laboratory experiments explored the impact of vegetation patchiness on channel-averaged turbulence and sediment transport. Stems were clustered into 16 randomly distributed circular patches of decreasing diameter. For the same channel velocity, the sediment transport increased with total stem number but decreased as stems were clustered into smaller patch diameters, occupying a smaller fraction of the bed area. The channel-averaged turbulence, which also declined with increased clustering, was shown to be a good predictor for sediment transport at the channel scale. Previous models for uniform vegetation were adapted to predict both the channel-averaged turbulence and sediment transport as a function of the total number of stems and degree of clustering, represented by the fraction of bed covered by patches. This provides a way for numerical modelers to represent the impact of subgrid-scale vegetation patchiness on sediment transport.

1. Introduction

Vegetation is often present in rivers and on floodplains, altering the velocity and turbulence intensity, which in turn alters sediment transport and bed morphology (e.g., Bywater-Reyes et al., 2018; Rominger et al., 2010; Sukhodolov & Sukhodolova, 2010; Yang & Nepf, 2019). Some channel restoration projects use vegetation to stabilize banks and floodplains (Surian et al., 2015; Tal & Paola, 2010), but to do so effectively, it is crucial to understand how vegetation impacts sediment transport (e.g., Larsen & Harvey, 2010; Reed et al., 1999). While vegetation can reduce local velocity, which promotes sediment retention, recent studies have highlighted how vegetation-generated turbulence may also enhance resuspension and sediment transport (Tinoco & Coco, 2016, 2018; Yager & Schmeeckle, 2013; Yang et al., 2016; Yang & Nepf, 2018). Further, when vegetation-generated turbulence is present, sediment transport models based on bed shear stress, τ, do not provide good estimates of sediment transport (Yager & Schmeeckle, 2013; Yang & Nepf, 2018). Recent studies have suggested that near-bed turbulence, k_t, may be a better predictor of sediment transport. For example, the initiation of both bed load and suspended load transport in vegetated channels can be better described by a threshold value of k_t than of τ (Tang et al., 2019; Tinoco & Coco, 2018; Yang et al., 2016).

The turbulent kinetic energy per fluid mass, k_t, includes bed-generated turbulence, $k_{t(bed)}$, and vegetation-generated turbulence, $k_{t(veg)}$. Bed-generated turbulence is correlated with the bed shear stress, $\tau = \rho C_f U^2$, with fluid density, ρ, velocity, U, and bed drag coefficient, C_f (e.g., Biron et al., 2004). Specifically, $k_{t(bed)} = \tau/\omega$, with scale factor $\omega = 0.20 \pm 0.01$ (Soulsby, 1981). Assuming a vegetation consisting of circular stems, the vegetation-generated turbulence, $k_{t(veg)}$, can be estimated from $k_t = \gamma^2 \left[\left(C_{D(form)} \frac{\phi}{1-\phi} \frac{2}{\pi}\right)^{2/3} U^2\right]$ (Tanino & Nepf, 2008a), in which γ is an empirical coefficient and φ is the solid volume fraction of the vegetation. Yang et al. (2016) and Yang and Nepf (2019) combined these two models to predict the total turbulence, k_t, in a channel with emergent vegetation:

$$k_t = \underbrace{\frac{C_f U^2}{\omega}}_{k_{t(bed)}} + \underbrace{\gamma^2 \left[\left(C_{D(form)} \frac{\phi}{1-\phi} \frac{2}{\pi}\right)^{2/3} U^2\right]}_{k_{t(veg)}} \quad (1)$$

Because only form drag contributes to turbulence generation, equation 1 uses a form drag coefficient, $C_{D(form)} = 2[(0.46 \pm 0.11) + (3.8 \pm 0.5)\,\phi]$, described for random arrays in Equation (2.10) in Tanino and Nepf (2008a). The second term in equation 1 is only valid when the stem wakes are turbulent, that is, $Re_d = Ud/\nu > 120$, with stem diameter d and kinematic viscosity ν (Liu & Nepf, 2016). Finally, equation 1 is valid for stem spacing greater than the stem diameter (Tanino & Nepf, 2008a).

The Einstein-Brown equation, based on measurements in a bare channel, provides an empirical description of bed load transport as a function of bed shear stress (Brown, 1950; Einstein, 1950). Yang and Nepf (2018) suggested that this relationship could be converted to a k_t-based model (equation 2 below) using the expression provided above ($k_{t(bed)} = \tau/\omega$). They verified that bed load transport rate per channel width, Q_s, could be predicted from near-bed turbulence in both vegetated and bare channels. Specifically, the nondimensional bed load transport, Q_{s*} ($= \frac{Q_s}{\rho_s\sqrt{(\rho_s/\rho - 1)gd_s{}^3}}$, in which ρ_s is the sediment density, d_s is the sediment diameter, and g is the acceleration of gravity), can be predicted from the nondimensional turbulence, k_{t*} ($= \frac{k_t}{(\rho_s/\rho - 1)gd_s}$):

$$Q_{s*} = \begin{cases} 2.15e^{\beta/k_{t*}}, & k_{t*} < 0.95 \\ 0.27{k_{t*}}^3, & 0.95 < k_{t*} < 2.74 \end{cases} \tag{2}$$

in which $\beta = -2.06$ is the original scale factor in the Einstein-Brown equation adapted by Yang and Nepf (2018) (see also Julien, 2010). Yang and Nepf (2018, 2019) validated the turbulence (equation 1) and bed load transport (equation 2) models using experiments with model vegetation consisting of staggered arrays of circular cylinders distributed uniformly across the channel width, for which the velocity averaged over distances greater than the stem spacing was uniform over the channel width (see Figures 4 and 5 in Yang & Nepf, 2019). However, in nature, vegetation often exists in individual patches of limited width and length. For example, the patch size in rivers has been observed to fall between 0.5 and 5 m, smaller than the channel width (e.g., Cornacchia et al., 2018; Sand-Jensen & Pedersen, 2008; Schoelynck et al., 2012). The horizontal distribution of patches is constrained by feedbacks between hydrodynamic, morphologic, and biologic processes, which often results in patches of vegetation within which velocity is lower separated by unvegetated regions in which the velocity is higher (e.g., Montgomery et al., 2018; Temmerman et al., 2007). The present study sought to understand how the patchy distribution of vegetation within a channel would influence bed load transport. A model was proposed to predict the spatial mean turbulence. The new turbulence model was combined with equation 2 to predict bed load transport.

2. Theory: Turbulence in a Channel With Patchy Vegetation

In this study, a heterogeneous distribution of vegetation will be represented by an idealized configuration of circular patches with bare channel between them. Consider M circular patches of vegetation, each of diameter D (gray circles in Figure 1) that are randomly distributed in an L-m-long and B-m-wide section of channel. The fraction of bed occupied by patches is $\phi_p = \frac{\pi MD^2}{4\,LB}$. It is used to describe the weighted average contribution of the patches to channel-averaged velocity and turbulence (see equations 3, 6, and 7, below). Within each patch, the vegetation is represented by a random distribution of cylindrical stems with diameter d and stem density m (stems/bed area), such that the solid volume fraction within the patch is $\phi = \frac{\pi}{4}md^2$, which is used to describe the in-patch turbulence generation (see equation 7 below). The channel-averaged solid volume fraction $\phi_c = \frac{\pi n_{total}}{4\,LB}d^2$ describes the total amount of vegetation in the channel, with n_{total} the total number of stems in the section $L \times B$.

A channel with patches of vegetation may have three sources of turbulence: bed shear, stem wake, and patch wake. The generation of turbulence within individual stem wakes has been observed for both vegetation mimics (rigid cylinders, Nepf & Vivoni, 2000; Poggi et al., 2004; Tanino & Nepf, 2008a) and real vegetation (King et al., 2012), and it occurs when the stem Reynolds number, $Re_d\left(= \frac{Ud}{\upsilon}\right)$, >120 (Liu & Nepf, 2016). Patch-scale vortices can form in the wake of a porous patch when $\varphi > 0.05$. Because the porosity of the patch allows bleed flow into the wake, the patch-scale vortices appear 5 to 10 diameters downstream from the patch (Nicolle & Eames, 2011; Zong & Nepf, 2012). The present study considered a distribution of patches spaced at distances of no more than six diameters, in which case the flow was redirected by neighboring patches before the patch wake developed vortices, so that patch-scale turbulence was not generated. This

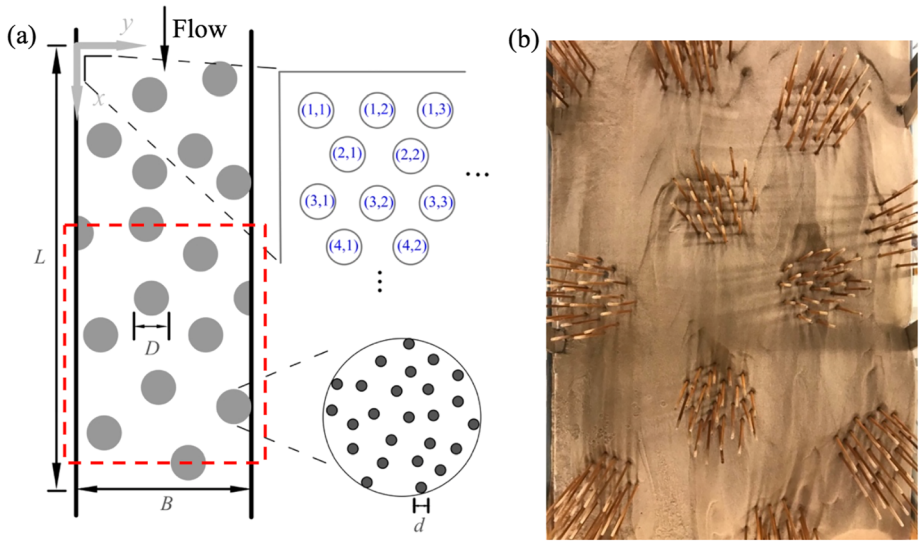

Figure 1. (a) Randomly distributed model vegetation patches in an L-m-long and B-m-wide channel section. Gray circles indicate patches within which cylinders were randomly distributed. The white area indicates bare sand bed. The individual cylinders were inserted into predrilled holes in the baseboard. The staggered array of holes was labeled with a coordinate system (c_x,c_y), a portion of which is shown in the inset above. Within the test section, $c_x = 1$ to 190 and $c_y = 1$ to 80. (b) Patch Case 2.4 (Table 1), in which each patch had a diameter $D = 20$ cm and contained 25 dowels. The photo shows the area denoted by a red dashed box in subplot (a), in which full and half patches were included.

was confirmed by flow visualization, which is described and illustrated in Figure S1 in the supporting information (SI). For this reason, patch-scale turbulence will not be considered here. The channel-averaged turbulent kinetic energy, $\langle k_t \rangle$, is defined as the area-weighted average of the turbulence generated in the bare channel and within the patches. The bracket denotes the spatial average.

Because the vegetation contributes to flow resistance, the average velocity within a patch, U_p, is smaller than the spatially averaged velocity in the bare channel, U_b. These velocities are related to the channel-averaged velocity, U_o, by the conservation of mass:

$$U_o = U_b\left(1 - \phi_p\right) + U_p\phi_p \tag{3}$$

U_p is defined as the average of the velocity entering, assumed to be U_b, and exiting, U_e, each patch; that is,

$$U_p = (U_b + U_e)/2 \tag{4}$$

The velocity exiting the patch, U_e, is estimated from the equation (5) in Chen et al. (2012), which describes the velocity exiting an individual patch:

$$\frac{U_e}{U_b} = 1 - \mu\frac{D}{L_p}, \tag{5}$$

in which $\mu = 0.42 \pm 0.03$. $L_p = \left[\left(\frac{2(1-\phi)}{C_D a}\right)^2 + \left(\frac{D}{2}\right)^2\right]^{1/2}$ is the flow adjustment length-scale within the patch (Rominger & Nepf, 2011), and a ($=md$) is the frontal area per volume inside the patch, and C_D is the drag coefficient, which is a function of φ and $Re_{d(p)} = U_p d/\upsilon$, as described for random cylinder distributions in Tanino and Nepf (2008b). Since U_p is required for $Re_{d(p)}$, an iterative solution of equations 3–5 is needed. Starting from $C_D = 1$, L_p was estimated and used to obtain U_e from equation 5, which in turn was used in equation 4 to estimate U_p. Next, $Re_{d(p)}$ ($=U_p d/\upsilon$) and φ were used to estimate a new C_D (Tanino & Nepf, 2008b). The iteration was repeated until consecutive estimates of C_D differed by less than 5%.

The bed-generated turbulence in equation 1 is modified to be a weighted average of the bare and patch regions, with φ_p defining the area occupied by vegetation. The channel-averaged bed-generated turbulence is then

$$k_{t(bed)} = \underbrace{\frac{C_f}{\omega} U_b{}^2 \left(1 - \phi_p\right)}_{bare\ channel} + \underbrace{\frac{C_f}{\omega} U_p{}^2 \phi_p}_{inside\ patches} \tag{6}$$

The stem turbulence is described by the second term in equation 1 using the patch velocity, U_p. The stem contribution to the channel average is then

$$\langle k_{t(veg)} \rangle = \gamma^2 \left[\left(C_{D(form)} \frac{\phi}{1-\phi} \frac{2}{\pi} \right)^{2/3} U_p{}^2 \right] \phi_p \tag{7}$$

Finally, the channel-averaged turbulent kinetic energy, $\langle k_t \rangle$, is the sum of equations 6 and 7.

3. Experimental Methods

Experiments were designed to explore how vegetation patchiness impacts bed load transport and to test the models for channel-averaged turbulence (equations 6 and 7) and bed load transport (equation 2). Vegetation clustering was increased by distributing the same number of stems into patches of smaller diameter, D, which resulted in a smaller value of φ_p, the fraction of bed covered by vegetation patches. That is, a higher clustering corresponded to smaller patch diameter. The experiments were performed in a 10-m-long and 1-m-wide flume with a horizontal bed, which recirculated water and sediment through separate pipes. The flow depth was $H = 12.0 \pm 0.4$ cm, and the channel-averaged velocity was $U_o = 30.0 \pm 0.5$ cm/s. The Reynolds number Re ($=U_oR/\upsilon$, with the hydraulic radius R) was 29,000, and the Froude number, Fr ($=U_o/\sqrt{gH}$), $= 0.3 < 1$, indicating that the flow was turbulent and subcritical.

The model vegetation consisted of circular cylinders arranged in randomly distributed patches (Figure 1) or in a uniform random distribution that covered the entire test section (Figure S2 in SI). The cylinders do not represent a specific macrophyte but resemble the morphology of a reed, the base of a tree, or a mangrove root (e.g., Lightbody & Nepf, 2006; Liu et al., 2018; Shan et al., 2019; Tinoco & Coco, 2016; Zhang et al., 2018). The cylinder diameter, $d = 0.6$ cm, was chosen based on the range of scales found in reeds and young plants on floodplains, $d = 0.2$ to 1.2 cm (e.g., Lightbody & Nepf, 2006; Manners et al., 2015). The cylinders extended through the water depth, modeling emergent vegetation. The channel-averaged solid volume fractions $\varphi_c = 0.005$, 0.015, and 0.02, were chosen based on the observed range in a reed bed, $\varphi_c = 0.001$ to 0.04 (Coon et al., 2000; Grace & Harrison, 1986). The Control Case 1.1 was with a bare bed, that is, no cylinders.

In each case with patches, $M = 16$ circular patches were randomly distributed within the test section (2.4 m × 1 m, Figure 1a). The patch diameter, D, was varied from 6.5 to 30 cm, resulting in patch area fractions $\varphi_p = 0.01$ to 0.24. The length of the test section was limited by the position of the sediment return. Because the flow adjusts to (deflects around) each patch, a fully developed flow was not present in the test section. Predrilled holes in the baseboards were used to determine the patch positions. The streamwise, lateral, and vertical directions were denoted as x, y, and z, respectively, with the origin at the right sidewall at the leading edge of the test section. The test section had $c_x = 1$ to 190 holes in the x direction and $c_y = 1$ to 80 holes in the y direction. The hole closest to the origin was $(c_x, c_y) = (1,1)$, as shown in Figure 1a. The center position (hole) of each patch was determined using the MATLAB random number generator. To avoid overlapping patches, a minimum distance of D was allowed between the centers of any two patches. Half patches were constructed if the distance between the patch center and the side wall was less than $D/2$. Patch distributions for Cases 2.1 to 4.3 (Table 1) are shown in Figures S3–S5 in SI. For the uniform random array, the position of each cylinder was randomly selected.

A 5-cm-thick layer of sand was placed on top of the baseboards and manually flattened. The mean sand grain diameter was $d_s = 0.5$ mm, and the sand density was $\rho_s = 2.65$ g/cm^3. The sediment transport rate was measured by using a T-valve to divert sediment from the recirculation pipe into a mesh bag for a measured collection time. The mesh bag was hung to drain and shook to remove excess water. The sand was then placed

Table 1
Summary of Experimental Parameters

Case pattern	Case	D (m)	m (m^{-2})	n_{total}	n_{patch}	φ_c	φ_p	φ	U_b (cm/s)	U_p (cm/s)	$Q_s \pm \sigma_{Q_s}$ (g/m/s)	$k_t \pm \sigma_{k_t}$ (cm^2/s^2)	$k_{t(max)}$ (cm^2/s^2)
Bare channel	1.1	—	—	0	0	0	—	—	30.0	30.0	0.20 ± 0.04	14 ± 1	—
Patches	2.1[a]	0.065	7,538	400	25	0.005	0.02	0.24	30.3	17.9	1.0 ± 0.3	23 ± 3	54
	2.2[a]	0.1	3,185	400	25	0.005	0.05	0.10	30.5	21.3	1.2 ± 0.3	21 ± 2	35
	2.3	0.15	1,415	400	25	0.005	0.12	0.05	30.7	24.8	1.9 ± 0.5	23 ± 3	97
	2.4[a]	0.2	796	400	25	0.005	0.21	0.03	31.0	26.5	1.6 ± 0.3	26 ± 4	92
	2.5[a]	0.3	354	400	25	0.005	0.47	0.01	32.1	27.9	2.5 ± 0.3	39 ± 5	96
	3.1	0.15	4,246	1,200	75	0.015	0.12	0.14	31.6	18.4	3.7 ± 1.0	25 ± 3	92
	3.2	0.2	2,389	1,200	75	0.015	0.21	0.08	32.7	20.2	5.2 ± 0.5	25 ± 3	81
	3.3	0.3	1,061	1,200	75	0.015	0.47	0.03	36.2	23.3	6.5 ± 0.4	32 ± 3	61
	4.1	0.2	3,185	1,600	100	0.02	0.21	0.10	33.0	18.8	4.6 ± 0.8	26 ± 3	85
	4.2	0.25	2,038	1,600	100	0.02	0.33	0.07	34.9	20.2	7.0 ± 0.6	30 ± 5	160
	4.3	0.3	1,415	1,600	100	0.02	0.47	0.05	37.8	21.6	9.8 ± 1.0	32 ± 3	86
Uniform random distribution	5.1	—	—	400	—	0.005	1	—	30.2	30.2	2.8 ± 0.6	25 ± 5	126
	5.2	—	—	1,200	—	0.015	1	—	30.5	30.5	8.4 ± 0.5	43 ± 3	62
	5.3	—	—	1,600	—	0.02	1	—	30.6	30.6	13 ± 1	48 ± 4	126

Note: D is the patch diameter; m is the cylinder density in the patch; n_{total} is the total number of cylinders in the test section; n_{patch} is the number of cylinders per patch; φ_c ($=\frac{\pi}{4}\frac{n_{total}}{LB}d^2$) is the channel-averaged solid volume fraction, with bed area LB and cylinder diameter d; φ_p ($=\frac{\pi}{4}nD^2$) is the patch area fraction, with $n = 6.67\ m^{-2}$ the number of patches per unit bed area; φ ($=\frac{\pi}{4}md^2$) is the solid volume fraction inside the patch; U_b and U_p are the spatial mean velocities in the bare channel and in a patch, respectively, using equations 3–5. Q_s is the sediment transport rate per channel width. $\langle k_t \rangle$ and $k_{t(max)}$ are the mean and maximum turbulent kinetic energy measured over two transects, respectively.
[a]Cases for which two realizations were performed with different patch distributions. For each patch case, sixteen circular patches were constructed in the test section.

into a container with 5 L of water, and the displacement of water provided a measure of the sediment volume (V) and mass ($\rho_s V$). The transport rate per unit channel width, Q_s ($g{\cdot}m^{-1}{\cdot}s^{-1}$), was calculated as the collected sand mass divided by the collection time and the width of the channel. Four replicate measurements were used to estimate the mean Q_s and standard error, σ_{Q_s}. This was repeated every 3 hr until the measured Q_s $\left(\pm\sigma_{Q_s}\right)$ was the same as the previous, indicating that the bed load transport had reached equilibrium, which required 14 to 30 hr of running time.

After transport equilibrium was achieved, a Nortek Vectrino with a side-looking probe was used to measure the instantaneous velocities $u(t)$, $v(t)$, and $w(t)$, corresponding to the (x,y,z) directions, respectively, along lateral transects with a 5-cm interval between measurements. The velocity was measured at mid-depth ($z = 6$ cm). Vertical profiles confirmed that measurements at mid-depth provided representative values of depth-averaged velocity (see Figure S6a in SI). Further, the mid-depth turbulence was similar to the near-bed turbulence (see Figure S6b). Specifically, the ratio of near-bed to mid-depth turbulence was 1.1 ± 0.3, indicating bedforms did not contribute significantly to turbulence. MATLAB code was used to extract time-averaged ($\overline{u}$, $\overline{v}$, and $\overline{w}$) and fluctuating (u', v', and w') velocities. The turbulent kinetic energy was defined as $k_t = 0.5\left(\overline{u'^2} + \overline{v'^2} + \overline{w'^2}\right)$. The noise in the velocity and turbulence measurements was 0.1 cm/s and 0.15 cm^2/s^2, respectively, determined from measurements in still water. For each condition, a lateral profile of velocities was measured at two streamwise positions. The channel-averaged turbulent kinetic energy was determined as the average over both transects, which was denoted as $\langle k_t \rangle$. A channel-averaged $\langle k_t \rangle$ based on eight transects differed by only 6% from one based on two transects, confirming that two transects was sufficient (Figure S7b in SI). The maximum value of turbulent kinetic energy within the two transects was denoted $k_{t(max)}$. For patchy cases, transects of time mean velocity and turbulent kinetic energy are summarized in Table S1 in SI.

4. Results and Discussion

The channel-averaged turbulent kinetic energy predicted from equations 6 and 7 was compared to the measured values (Figure S8a in SI). The bed drag coefficient was $C_f = 0.004 \pm 0.001$, based on $C_f = [5.75\log(2H/$

$d_s)]^{-2}$ from Julien (2010). The scale coefficient $\omega = 0.22 \pm 0.01$ was determined from the bare bed condition (green dot in Figure S8a), which was consistent with previous estimates (0.20 ± 0.01 in Soulsby, 1981). The scale constant $\gamma = 0.8 \pm 0.4$ (95% CI) was determined using a least squares fit of predicted $\langle k_t \rangle$ to measured values from all cases in Table 1. This value was consistent with previous measurements in uniform random arrays ($\gamma = 1.1$, Tanino & Nepf, 2008a). Note that Yang and Nepf (2019) fit a slightly smaller value ($\gamma = 0.6$) to measurements of turbulence in uniform staggered arrays, suggesting that staggered arrays produce slightly less turbulence, possibly due to the influence of upstream, in-line wakes.

The predicted turbulent kinetic energy was used to predict the sediment transport rate, equation 2, which was then fit to the measured sediment transport rate (Table 1) with $\beta = -1.6 \pm 0.3$ (Figure S8 in SI). The combined prediction of $\langle k_t \rangle$ (equations 6 and 7) and Q_s (equation 2) worked across all cases with randomly arranged cylinders (this study, Figure S8b) and for most cases with staggered cylinders from Yang and Nepf (2019, diamonds in Figure S8b) with similar flow depth h (=10 to 12 cm), channel velocity U_o (=21 to 43 cm/s), and sediment size (0.5 mm) to this study. An overprediction in staggered arrays was noted at low values of sediment transport. This is likely due to the fact that the turbulence model used here (with $\gamma = 0.8$) over predicted the turbulence in the staggered array (with $\gamma = 0.6$), and the overprediction of $\langle k_t \rangle$ contributed to an overprediction of Q_s.

For each channel-averaged stem density (φ_c), the bed load transport was highest for the uniform, random distribution (blue dots in Figure 2) and decreased as patches formed and decreased in size (Figures 2a, 2c, and 2e). The sediment transport rate was highest and the impact of clustering (decreasing patch size) was greatest for the highest channel-averaged stem density ($\varphi_c = 0.02$, Figure 2e). The trends in Q_s were generally consistent with the trends in measured turbulence. Specifically, for $\varphi_c = 0.015$ and 0.02, the peak turbulence was associated with the uniform random distribution and turbulence level decreased as patches formed and decreased in size. The smallest bed load transport rate and turbulence level were observed in the bare channel (green points in Figures 2a and 2b).

By describing the relative contributions of bed- and vegetation-generated turbulence, equations 6 and 7 provided insight into the changes in bed load transport associated with changes in the total number of stems and patch size. Specifically, the trends in turbulence, and by association in sediment transport, were due mostly to changes in vegetation-generated turbulence. As the stem distribution changed, the bed-generated turbulence ($\langle k_{t(bed)} \rangle$, orange dashed lines in Figure 2) had almost no change (<5%), whereas the vegetation-generated turbulence ($\langle k_{t(veg)} \rangle$, blue dashed lines) approximately tripled between the smallest patch size (smallest φ_p) and the uniform random distribution. The relative contributions of bed- and vegetation-generated turbulence also depended on the total amount of vegetation present. For example, for the randomly distributed stems at the smallest channel-averaged stem density ($\varphi_c = 0.005$), the vegetation-generated turbulence was smaller than the bed-generated turbulence (Figure 2b). Because of this, clustering the vegetation into patches did not have a significant impact on channel-averaged turbulence (Figure 2b) or bed load transport (Figure 2a). In contrast, for the higher stem densities ($\varphi_c = 0.015$ and 0.02), vegetation-generated turbulence exceeded bed-generated turbulence in the random distribution, so that when clustering was introduced, the drop in vegetation-generated turbulence had a significant impact on channel-averaged turbulence (Figures 2d and 2f) and bed load transport (Figures 2c and 2e). The clustering of vegetation into patches decreased the velocity impacting individual stems, which decreased the stem-generated turbulence (equation 7). Specifically, as the patches became more clustered (smaller D and higher φ), the velocity within the patch, U_p, declined (Table 1). The decrease in U_p could be more pronounced if the patch was placed directly in the wake of the upstream patch (e.g., Ghani et al., 2019). In addition, as clustering increased (decreasing D), a smaller fraction of bed area contained patches (smaller φ_p). These two trends led to a decline in $\langle k_{t(veg)} \rangle$.

The variation in measured bed load transport, Q_s, exhibited a dependence on channel-averaged turbulence, but no dependence on channel-averaged bed shear stress, which was estimated as $\langle \tau \rangle = C_f U_b^2 (1 - \varphi_p) + C_f U_p^2 \varphi_p$ (Figure 3). The bed load transport increased with increasing $\langle k_t \rangle$, but had no clear dependence on $\langle \tau \rangle$. Specifically, across the range of patch conditions, the bed shear stress was unchanged within uncertainty, yet the bed load transport exhibited a more than tenfold change (Figure 3b and Table 1). Further, the bed load transport had little dependence on peak turbulence, $k_{t(max)}$, because $k_{t(max)}$ did not vary

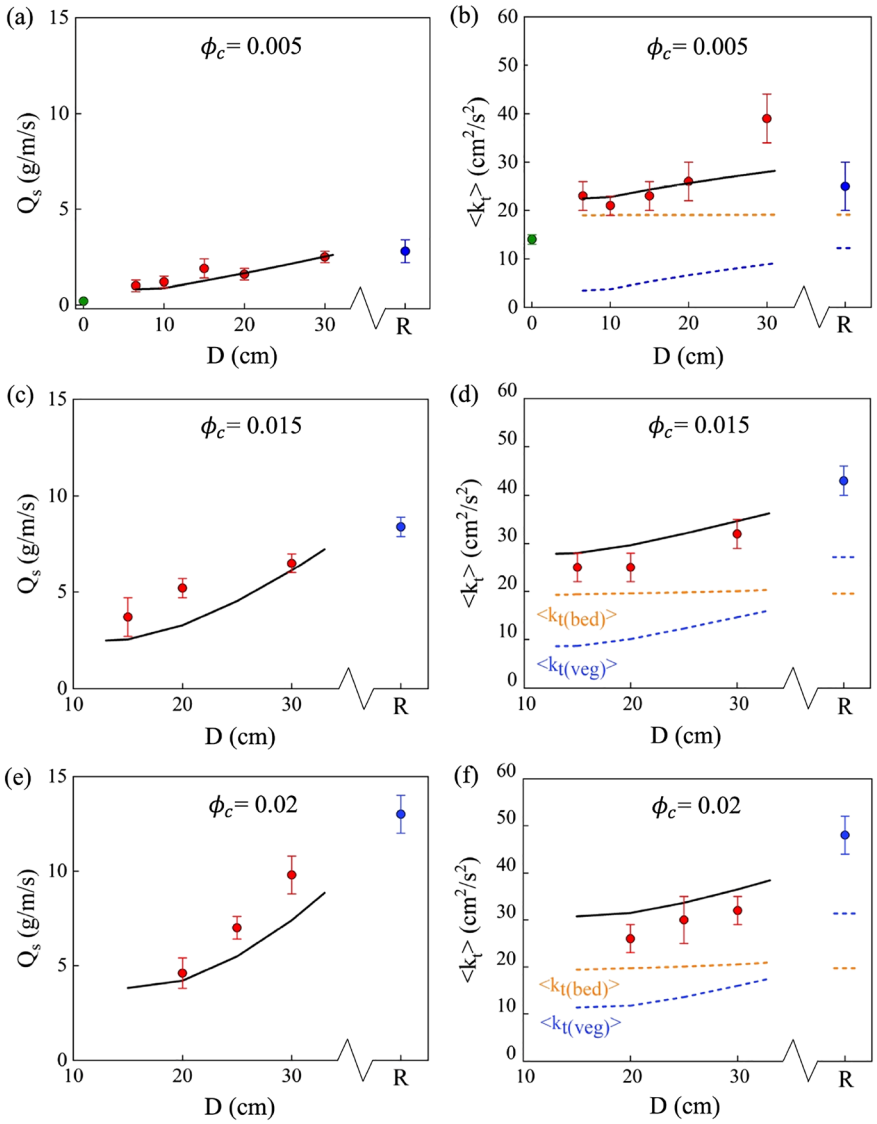

Figure 2. (a, c, and e) Measured (red symbols) and predicted (solid curve, equations 2, 6, and 7) bed load transport, Q_s, as a function of patch diameter, D. (b, d, and f) Measured (red symbols) and predicted (equations 6 and 7) channel-averaged turbulent kinetic energy, $\langle k_t \rangle$.$\langle k_{t(bed)} \rangle$is predicted from equation 6 using $C_f = 0.004$, U_b, U_p, and φ_p (orange dashed line), and$\langle k_{t(veg)} \rangle$is predicted from equation 7 using $\gamma = 0.8$, φ, U_p, and φ_p (blue dashed lines). All parameters are summarized in Table 1. The blue symbols above the axis label "R" indicate uniform random distributions ($\varphi_p = 1$). The red symbols indicate randomly distributed patches. The green symbols in (a) and (b) indicate the bare channel case. Channel-averaged solid volume fraction are (a, b) $\phi_c = 0.005$, (c, d) $\phi_c = 0.015$, and (e, f) $\phi_c = 0.02$.

consistently with the spatial average $\langle k_t \rangle$. Specifically, $k_{t(max)}/\langle k_t \rangle$ exhibited a wide range of value (between 1.4 and 5.4) that did not vary systematically with either the channel-scale vegetation density, φ_c, or the fraction of channel occupied by vegetation patches, φ_p (see Figure S9 in SI). In order to impact the channel-averaged sediment transport directly, $k_{t(max)}$ would need to occur over a spacing smaller than or equal to the individual sediment excursions. It appears that this condition was not met in our study.

In modeling applications, it is convenient to assume a uniform distribution of vegetation within each grid cell (Δx), assigning a single grid-scale vegetation density, $\phi_c = \frac{\pi}{4}\frac{Nd^2}{\Delta x^2}$, with N the number of stems per grid cell. However, this study showed that heterogeneous distributions of vegetation, specifically the clustering of vegetation into discrete patches, can decrease turbulence and sediment transport, relative to a uniform stem distribution. To provide guidance to modelers, equations 2, 6, and 7 were used to explore the impact of

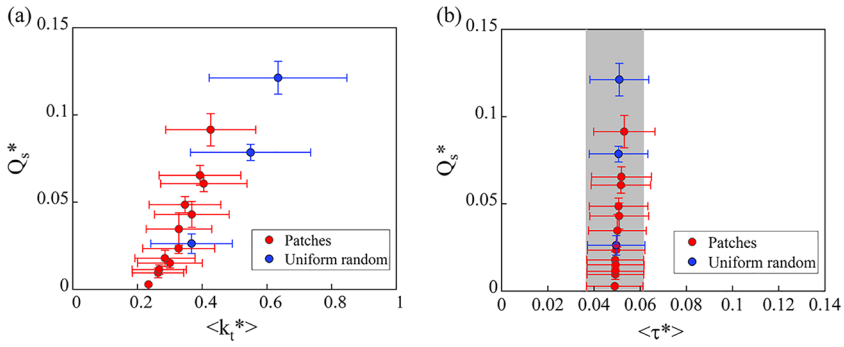

Figure 3. Measured sediment transport rate, $Q_{s*} = \frac{Q_s}{\rho_s\sqrt{(\rho_s/\rho-1)gd_g^3}}$, versus (a) channel-averaged turbulent kinetic energy, $\langle k_t^* \rangle = \frac{k_t}{(\rho_s/\rho-1)gd_g}$, from equations 6 and 7; and versus (b) channel-averaged bed shear stress, $\langle \tau^* \rangle = \frac{\tau}{(\rho_s/\rho-1)gd_g}$, with $\langle\tau\rangle = C_f U_b^2(1-\varphi_p) + C_f U_p^2 \varphi_p$. The vertical gray bar denotes $\langle\tau\rangle = C_f U_0^2$ with bar width indicating the uncertainty due to the propagated uncertainty of C_f and U_o. Patch cases are shown with red circles, and uniform random distributions are shown with blue circles.

vegetation patchiness over a larger parameter space. The values of $\langle k_t \rangle$ and Q_s predicted with randomly distributed patches ($\varphi_p < 1$) were normalized by the values predicted with uniform random distribution, $\varphi_p = 1$, which were labeled *UR*, that is, $\langle k_t \rangle_{UR}$ and $Q_{s\text{-}UR}$. The normalized values were plotted against the patch area fraction φ_p in a channel with randomly distributed patches (Figure 4). The magnitude of φ_p (<0.56) was restricted by the condition that overlapping patches were not allowed. The uniform random distribution produced the highest level of turbulence and bed load transport, so that $\langle k_t \rangle / \langle k_t \rangle_{UR}$ and $Q_s / Q_{s\text{-}RU}$ were always smaller than one. Both turbulence and bed load transport decreased as patch area became smaller (decreasing φ_p). Further, the impact of patch clustering became more important with increasing channel-averaged stem density (φ_c). This reinforces the point that when bed load sediment is simulated in vegetated channels, both vegetation clustering and density should be considered.

In natural systems, patches of vegetation are often shaped by feedbacks between flow, bed forms, and vegetation, which can result in vegetation distributions that tend toward highly channelized flows between patches (e.g., Kondziolka & Nepf, 2014; Larsen & Harvey, 2010; Montgomery et al., 2018; Yamasaki et al., 2019). Despite having an idealized circular patch geometry, a key result of this study can be transferred to more natural distributions of vegetation. The organization of vegetation into patches of sufficient density to deflect flow away from the vegetation leads to a decrease in vegetation-generated turbulence, which in turn leads to a decrease in channel-averaged sediment transport. This process is also relevant to vegetation organized into distributions of elongated vegetation patches separated by channelized flow, and the trends displayed in Figure 4 will also apply for this spatial distribution of vegetation, and it is similarly relevant to modeling if it occurs at the subgrid scale.

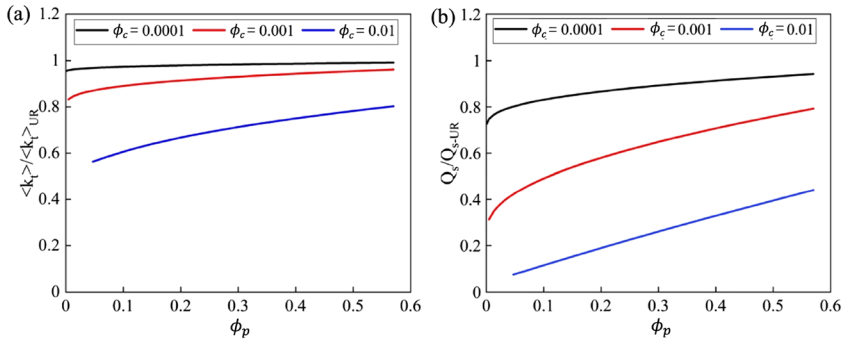

Figure 4. (a) Channel-averaged turbulence with randomly distributed patches, $\langle k_t \rangle$, normalized by the value for a uniform random distribution $\langle k_t \rangle_{UR}$, based on equations 6 and 7. (b) Channel-averaged bed load transport with randomly distributed patches, Q_s, normalized by the value for a uniform random distribution, $Q_{s\text{-}UR}$, based on equations 2, 6, and 7.

5. Summary

This study measured sediment transport in a channel with model vegetation and considered both uniform random distributions of individual stems and heterogeneous distributions with stems clustered into patches separated by bare bed. For the same channel velocity, the highest turbulence and bed load transport was observed with the uniform random distribution, and both turbulence and bed load transport decreased as stems were clustered into progressively smaller patch diameters, associated with a smaller fraction of bed area occupied by stems (smaller φ_p). For both uniform and clustered distributions of model vegetation the channel-averaged turbulence was shown to be a better predictor for sediment transport than channel-averaged bed shear stress. A model was developed to predict the channel-averaged turbulence and sediment transport as a function of channel-averaged vegetation density (φ_c) and degree of clustering, represented by vegetation patch area fraction (φ_p). This provides a way for numerical modelers to represent the impact of subgrid-scale heterogensity in vegetation distribution on sediment transport.

Acknowledgments
Y. Shan was funded by the NSFC (Grant 51709022) and the China Scholarship Council. C. Liu was funded by the NSFC (Grant 51879175) and the Huo Hua Ku Program of Sichuan University (2018SCUH0020). This research was supported by U.S. NSF Grant EAR 1854564. Any opinions, findings, and conclusions expressed are those of the author(s) and do not necessarily reflect the views of the National Science Foundation. All data presented in the paper are available through Figshare at this site (https://doi.org/10.6084/m9.figshare.12039711.v2).

References

Biron, P., Robson, C., Lapointe, M., & Gaskin, S. (2004). Comparing different methods of bed shear stress estimates in simple and complex flow fields. *Earth Surface Processes and Landforms: The Journal of the British Geomorphological Research Group*, *29*(11), 1403–1415. https://doi.org/10.1002/esp.1111

Brown, C. (1950). Sediment transportation. *Engineering Hydraulics*, *12*, 769–857.

Bywater-Reyes, S., Diehl, R., & Wilcox, A. (2018). The influence of a vegetated bar on channel-bend flow dynamics. *Earth Surface Dynamics*, *6*(2), 487–503. https://doi.org/10.5194/esurf-6-487-2018

Chen, Z., Ortiz, A., Zong, L., & Nepf, H. (2012). The wake structure behind a porous obstruction and its implications for deposition near a finite patch of emergent vegetation. *Water Resources Research*, *48*, W09517. https://doi.org/10.1029/2012WR012224

Coon, W., Bernard, J., & Seischab, F. (2000). *Effects of a cattail wetland on water quality of Irondequoit Creek near Rochester*, New York (no. 2000–4032). US Geological Survey.

Cornacchia, L., Van De Koppel, J., Van Der Wal, D., Wharton, G., Puijalon, S., & Bouma, T. J. (2018). Landscapes of facilitation: How self-organized patchiness of aquatic macrophytes promotes diversity in streams. *Ecology*, *99*(4), 832–847. https://doi.org/10.1002/ecy.2177

Einstein, H. (1950). *The bed-load function for sediment transportation in open channel flows (Technical Bulletin No 1026)*. Washington, DC: US Department of Agriculture.

Ghani, U., Anjum, N., Pasha, G. A., & Ahmad, M. (2019). Investigating the turbulent flow characteristics in an open channel with staggered vegetation patches. *River Research and Applications*, *35*(7), 966–978. https://doi.org/10.1002/rra.3460

Grace, J., & Harrison, J. (1986). The biology of Canadian weeds. Typha latifolia L., Typha angustifolia, L., and Typha xglauca Godr. *Canadian Journal of Plant Science*, *66*, 361–337. https://doi.org/10.4141/cjps86-051

Julien, P. (2010). *Erosion and sedimentation*, (2nd ed.p. 198). New York: Cambridge University Press.

King, A. T., Tinoco, R. O., & Cowen, E. A. (2012). A k–ε turbulence model based on the scales of vertical shear and stem wakes valid for emergent and submerged vegetated flows. *Journal of Fluid Mechanics*, *701*, 1–39. https://doi.org/10.1017/jfm.2012.113

Kondziolka, J., & Nepf, H. (2014). Vegetation wakes and wake interaction shaping aquatic landscape evolution. *Limnology and Oceanography: Fluids and Environments*, *4*, 1–14. https://doi.org/10.1215/21573689-2846314

Larsen, L., & Harvey, J. (2010). How vegetation and sediment transport feedbacks drive landscape change in the Everglades and wetlands worldwide. *The American Naturalist*, *176*(3), E66–E79. https://doi.org/10.1086/655215

Lightbody, A., & Nepf, H. (2006). Prediction of velocity profiles and longitudinal dispersion in emergent salt marsh vegetation. *Limnology and Oceanography*, *51*(1), 218–228. https://doi.org/10.4319/lo.2006.51.1.0218

Liu, C., Hu, Z., Lei, J., & Nepf, H. (2018). Vortex structure and sediment deposition in the wake behind a finite patch of model submerged vegetation. *Journal of Hydraulic Engineering*, *144*(2), 04017065. https://doi.org/10.1061/(ASCE)HY.1943-7900.0001408

Liu, C., & Nepf, H. (2016). Sediment deposition within and around a finite patch of model vegetation over a range of channel velocity. *Water Resources Research*, *52*, 600–612. https://doi.org/10.1002/2015WR018249

Manners, R., Wilcox, A., Kui, L., Lightbody, A., Stella, J., & Sklar, L. (2015). When do plants modify fluvial processes? Plant-hydraulic interactions under variable flow and sediment supply rates. *Journal of Geophysical Research: Earth Surface*, *120*, 325–345. https://doi.org/10.1002/2014JF003265

Montgomery, J. M., Bryan, K. R., Horstman, E. M., & Mullarney, J. C. (2018). Attenuation of tides and surges by mangroves: Contrasting case studies from New Zealand. *Watermark*, *10*(9), 1119. https://doi.org/10.3390/w10091119

Nepf, H. M., & Vivoni, E. R. (2000). Flow structure in depth-limited, vegetated flow. *Journal of Geophysical Research*, *105*(C12), 28,547–28,557. https://doi.org/10.1029/2000JC900145

Nicolle, A., & Eames, I. (2011). Numerical study of flow through and around a circular array of cylinders. *Journal of Fluid Mechanics*, *679*, 1–31. https://doi.org/10.1017/jfm.2011.77

Poggi, D., Porporato, A., Ridolfi, L., Albertson, J. D., & Katul, G. G. (2004). The effect of vegetation density on canopy sub-layer turbulence. *Boundary-Layer Meteorology*, *111*, 565–587. https://doi.org/10.1023/B:BOUN.0000016576.05621.73

Reed, D., Spencer, T., Murray, A., French, J., & Leonard, L. (1999). Marsh surface sediment deposition and the role of tidal creeks: Implications for created and managed coastal marshes. *Journal of Coastal Conservation*, *5*(1), 81–90. https://doi.org/10.1007/BF02802742

Rominger, J., Lightbody, A., & Nepf, H. (2010). The effects of vegetation on sand bar stability and stream hydrodynamics. *Journal of Hydraulic Engineering*, *136*(12), 994–1002. https://doi.org/10.1061/(ASCE)HY.1943-7900.0000215

Rominger, J., & Nepf, H. (2011). Flow adjustment and interior flow associated with a rectangular porous obstruction. *Journal of Fluid Mechanics*, *680*, 636–659. https://doi.org/10.1017/jfm.2011.199

Sand-Jensen, K., & Pedersen, M. (2008). Streamlining of plant patches in streams. *Freshwater Biology*, *53*(4), 714–726. https://doi.org/10.1111/j.1365-2427.2007.01928.x

Schoelynck, J., De Groote, T., Bal, K., Vandenbruwaene, W., Meire, P., & Temmerman, S. (2012). Self-organized patchiness and scale-dependent bio-geomorphic feedbacks in aquatic river vegetation. *Ecography*, *35*(8), 760–768. https://doi.org/10.1111/j.1600-0587.2011.07177.x

Shan, Y., Chao, L., & Nepf, H. (2019). Comparison of drag and velocity in model mangrove forests with random and in-line tree distributions. *Journal of Hydrology*, *568*, 735–746. https://doi.org/10.1016/j.jhydrol.2018.10.077

Soulsby, R. (1981). Measurement of the Reynolds stress components close to a marine sand bank. *Marine Geology*, *42*, 35–47. https://doi.org/10.1016/0025-3227(81)90157-2

Sukhodolov, A., & Sukhodolova, T. (2010). Case study: Effect of submerged aquatic plants on turbulence structure in a lowland river. *Journal of Hydraulic Engineering*, *136*(7), 434–446. https://doi.org/10.1061/(ASCE)HY.1943-7900.0000195

Surian, N., Barban, M., Ziliani, L., Monegato, G., Bertoldi, W., & Comiti, F. (2015). Vegetation turnover in a braided river: Frequency and effectiveness of floods of different magnitude. *Earth Surface Processes and Landforms*, *40*(4), 542–558. https://doi.org/10.1002/esp.3660

Tal, M., & Paola, C. (2010). Effects of vegetation on channel morphodynamics: Results and insights from laboratory experiments. *Earth Surface Processes and Landforms*, *35*, 1014–1028. https://doi.org/10.1002/esp.1908

Tang, C., Lei, J., & Nepf, H. (2019). The impact of a vegetation-generated turbulence on the critical wave-velocity for sediment resuspension. *Water Resources Research*, *55*, 5904–5917. https://doi.org/10.1029/2018WR024335

Tanino, Y., & Nepf, H. (2008a). Lateral dispersion in random cylinder arrays at high Reynolds number. *Journal of Fluid Mechanics*, *600*, 339–371. https://doi.org/10.1017/S0022112008000505

Tanino, Y., & Nepf, H. M. (2008b). Laboratory investigation of mean drag in a random array of rigid, emergent cylinders. *Journal of Hydraulic Engineering*, *134*(1), 34–41. https://doi.org/10.1061/(ASCE)0733-9429(2008)134:1(34

Temmerman, S., Bouma, T. J., Van de Koppel, J., Van der Wal, D., De Vries, M. B., & Herman, P. M. J. (2007). Vegetation causes channel erosion in a tidal landscape. *Geology*, *35*(7), 631–634. https://doi.org/10.1130/G23502A.1

Tinoco, R., & Coco, G. (2016). A laboratory study on sediment resuspension within arrays of rigid cylinders. *Advances in Water Resources*, *92*, 1–9. https://doi.org/10.1016/j.advwatres.2016.04.003

Tinoco, R. O., & Coco, G. (2018). Turbulence as the main driver of resuspension in oscillatory flow through vegetation. *Journal of Geophysical Research: Earth Surface*, *123*(5), 891–904. https://doi.org/10.1002/2017JF004504

Yager, E., & Schmeeckle, M. (2013). The influence of vegetation on turbulence and bed load transport. *Journal of Geophysical Research: Earth Surface*, *118*, 1585–1601. https://doi.org/10.1002/jgrf.20085

Yamasaki, T., Lima, P., Silva, D., de Preza, A., Janzen, J., & Nepf, H. (2019). From patch scale to channel scale: The evolution of emergent vegetation in a channel. *Advances in Water Resources*, *129*, 131–145. https://doi.org/10.1016/j.advwatres.2019.05.009

Yang, J. Q., Chung, H., & Nepf, H. M. (2016). The onset of sediment transport in vegetated channels predicted by turbulent kinetic energy. *Geophysical Research Letters*, *43*(21), 11–261. https://doi.org/10.1002/2016GL071092

Yang, J. Q., & Nepf, H. (2018). A turbulence-based bed-load transport model for bare and vegetated channels. *Geophysical Research Letters*, *45*(19), 10–428. https://doi.org/10.1029/2018GL079319

Yang, J. Q., & Nepf, H. (2019). Impact of vegetation on bedload transport rate and bedform characteristics. *Water Resources Research*, *55*, 6109–6124. https://doi.org/10.1029/2018WR024404

Zhang, Y., Tang, C., & Nepf, H. (2018). Turbulent kinetic energy in submerged model canopies under oscillatory flow. *Water Resources Research*, *54*, 1734–1750. https://doi.org/10.1002/2017WR021732

Zong, L., & Nepf, H. M. (2012). Vortex development behind a finite porous obstruction in a channel. *Journal of Fluid Mechanics*, *691*, 368–391. https://doi.org/10.1017/jfm.2011.479

References From the Supporting Information

Chen, D., & Jirka, G. (1995). Experimental study of plane turbulent wakes in a shallow water layer. *Fluid Dynamics Research*, *16*(1), 11–41. https://doi.org/10.1016/0169-5983(95)00053-G